Thermomechanical Characterization of Thermoplastic Polyimide to Improve the Chain Interaction via Crystalline Domains

Alejandro Rivera Nicholls,[1] Garrett Craft,[1] Yesenia Perez,[1] Matthew Pellissier,[1] John A. Stock,[1] Maxime Testemale,[2] Ken Kull,[1] Jarrod Eubank,[3] Julie P. Harmon[1]

[1]*University of South Florida, Tampa, Florida, 33620*
[2]*Sigma Clermont, 63178, Aubière, France*
[3]*Florida Southern College, Lakeland, Florida, 33801*

In a previous study on polyimides, we incorporated an aromatic diamine monomer with a methylene linker, 4,4′-methylenebis (2,6-dimethylaniline), to make a robust main chain along with aliphatic polyetherdiamine backbone linkers to decrease rigidity. In this report, we explore the behavior of crystalline regions provided by the organized packing of polyethylene oxide into the formerly characterized polymers. The polymers were designed to exhibit thermal properties in between those of conventional aromatic polyimides and polymers with wholly aliphatic ether diamine links, with a target to improve the mechanical characteristics. Through dynamic mechanical analysis and differential scanning calorimetry, it is shown that the incorporation of polyethylene oxide diamine and the removal of methyl pending groups serve to improve the organized packing of the chains. All of this allows for a broader range in tenability of thermal and mechanical properties of the polyimide. Furthermore, the crystalline regions are an important component to maintain the temperature stability of polyimide while maintaining the processability. The polymers are characterized by Fourier-transform infrared spectroscopy, thermomechanical and calorimetric analysis, microhardness measurements, tensile testing, and wide-angle X-ray scattering. POLYM. ENG. SCI., 59:1919–1932, 2019. © 2019 Society of Plastics Engineers

INTRODUCTION

Highly ordered aromatic backbones allow polyimides (PIs) to have superb properties demonstrated by elevated thermal stability, solvent resistance, low coefficients of thermal expansion, low dielectric constants, high glass transition temperatures, and superior mechanical properties [1–5]. These characteristics make them a sustainable option in the production of high performance products found in electronics, aerospace structural components, thermal insulation, composites, and adhesives [6–8]. The sizeable number of monomer combinations and the different synthetic methods [9–13] allow for their properties to be tailored depending on the suitable application, but it comes at a monetary cost compared to other polymer classes. Hence, the chemistry of polyimides is rather diverse with a variety of usable monomers and several methodologies available for synthesis.

The elevated energy cost to process these highly stable materials is due to high glass transition and melt temperatures, which range close to their decomposition temperatures [5, 7, 14–16]. Film coating is a common manufacturing process that involves a slurry of polyamic acid that is cured and imidized. This process can be subject to solvolysis or hydrolysis before the ring closure imidization [17, 18]. The process is great for the manufacturing of thin films, but it will encounter some limitations when processing complex shapes, which will require an external filling or a backbone modification. To by-pass the manufacturing hurdles, different groups have taken the initiative to make the polymers behave like conventional thermoplastics. To do so, the common procedure is to break the aromaticity of the backbone [6, 9, 19–23] by increasing flexibility and decreasing the different thermal transitions. To substantially lower the glass transition temperature, it is important to incorporate aliphatic linkers as it was demonstrated by Baldwin et al. [24], which introduced an entirely aliphatic ether as the diamine and reacted it with pyromellitic dianhydride (PMDA), reducing the glass transition temperature significantly (51°C–75°C). Otherwise, the T_g remains elevated, ranging from 215°C to over 310°C [6, 20–22], as most of the groups have shown with their respective backbone modifications. Although these materials can be processed before decomposition, the temperature requirements remain elevated and reprocessing or recycling is unlikely. As the number of aliphatic linkers is increased, the flexibility of the backbone is improved, and therefore the movement of the chains starts at a lower temperature [24]. The approach presented by our group [19] presents a series of polyimides that were designed to have tractable T_g using 4,4′-methylenebis (2,6-dimethylaniline) (MBDMA) with a wider range of glass transition temperatures (22°C–101°C). The flexibility introduced by the polypropylene oxide monomers influences the outstanding thermal properties that polyimides are recognized for. The decrease in the order of the backbone increases the solubility in previously used solvents like m-cresol, gamma-butyrolactone, and n-methyl pyrrolidone among others. This becomes an issue in the current applications because the polymer will lose its structure and collapse in the performance. The collaboration among the chains needs to be increased to promote more stable properties for the polyimides previously explored [19].

There are different options to improve the interaction of the chains and improve the properties of a polymer. These vary from the most extreme chemical crosslinking that turn the polymer into a thermoset, to reversible physical crosslinking influenced by an external factor, and finally a closer packing of the chains that could create organized lattices. Crystalline regions in the polymer can provide some interaction between the chains that influences the thermomechanical properties of the polymer [25]. Aromatic polyimides commonly have large crystalline regions due to their repetitive monomers and compatibility of the structures. The usage of two aromatic monomers provides the possibility for the entire material to be uniform and allows it to lock into an organized conformation. When a third monomer is introduced, the

Correspondence to: J.P. Harmon; e-mail: harmon@usf.edu
DOI 10.1002/pen.25194
Published online in Wiley Online Library (wileyonlinelibrary.com).

pattern is disrupted and the crystallinity is affected. With the addition of an aliphatic polypropylene oxide diamine [19], the length uniformity between the aromatic monomers of the chains is altered. Also, the polypropylene oxide has a small methyl-pending group that acts as a protuberance and prevents a tight packing of the backbone. Polyethylene oxide evidences tighter packing of the chains and creates defined crystal structures [26–30]. The packing of the chains influences the behavior of the polymer because the energy required to move the chains increases and renders the polymer more thermally stable polymer. When polyimides have flexible backbones [19, 24] their thermal transitions are lowered and they lose the superb characteristics that they are valued for. Polyurethanes [25] are a class of polymers that can have lower transition temperatures, but with the aid of crystalline regions, they can perform well at higher temperatures. Herein we explore the introduction of the crystalline regions in a series of flexible polyimides that could improve the properties that were diminished when the flexible monomer was introduced.

The Jeffamines® D series polyols based on a propylene oxide backbone are replaced with the Jeffamine® EDR series, which is based on a polyethylene oxide backbone exhibiting crystallinity [26–30]. In this material, the overall polymer does not crystallize, but there some localized regions that crystallize to hold the polyimide chains together above the T_g. The objective of this modification is to maintain the lower temperature processability achieved with the aliphatic diamine but recover the thermomechanical properties to compete with commercially available products like Kapton® or Vespel® characteristics. The polymers were characterized by FTIR, GPC, thermomechanical and calorimetric analysis, tensile testing, microhardness testing, and WAXS.

MATERIALS AND METHODS

Materials

3,3′,4,4′-Benzophenonetetracarboxylic dianhydride (BTDA), pyromellitic dianhydride (PMDA), 4,4′-methylenebis (2,6-dimethylaniline) (MBDMA), and gamma-butyrolactone (GBL) were used as received and donated by BrightVolt, Inc. (Lakeland, FL) [31, 32]. Jeffamine® D230 (short polypropylene-oxide diamine, SPPO), and EDR148 (polyethylene-oxide diamine, PEO), were donated by Huntsman, Inc. (The Woodlands, TX). HPLC-grade tetrahydrofuran (THF) was used as received from Sigma–Aldrich. Narrow molecular weight polystyrene standards were purchased from Fluka Analytical.

Methods

General Procedure for Polymerization. Polyimides with varying stoichiometric ratios of aliphatic amines monomers (Table 1), were synthesized via a condensation polymerization (Fig. 1). In each reaction, approximately 250 g of polyimides were synthesized. First, the reaction apparatus, consisting of a four-necked glass reactor, a heating mantle, a mechanical mixer, a nitrogen line, a thermocouple and distillation head, was set up. The 1 L reactor was charged with the appropriate mixture of amines (polyethylene-oxide diamine (PEO), short polypropylene-oxide diamine (SPPO), and MBDMA) and blended using the mechanical mixer with Teflon blades. The mixture was warmed at 30°C for 20 min until it was thoroughly homogenized by using the mixer. Subsequently, a dianhydride monomer (BTDA or PMDA) was dissolved in GBL and added to the reactor to start the polymerization. Thereafter, the temperature was incremented to 80°C and kept under inert conditions with N_2 for 24 h. The water formed by the closure of the imidization ring of the polyamic acid and surplus of GBL was vacuum distilled. The mixture was kept under vacuum for the remainder of the reaction until the solvent evaporated. The polyimide slurry yielded from the reaction was transferred into a Teflon pan and oven cured at 200°C for 2 h to completely close the imidization ring. Then, it was stored in a vacuum oven at 100°C to further dry the product.

Fourier Transform Infrared Spectroscopy/Attenuated Total Reflectance. Thin film samples were prepared in a heated Carver hydraulic press. The films were analyzed conducting 16 scans from 400 to 4,000 cm^{-1} at room temperature using a Spectrum One FT-IR (Perkin Elmer) equipped with ATR. The resulting data was collected in reflection mode and it was analyzed using the Spectrum software [33, 34].

Gel Permeation Chromatography. Solutions with a concentration of 5 mg per mL were created by dissolving a specific amount of each sample into tetrahydrofuran (THF) and filtered with 0.2 μm PTFE syringe filters. The analysis of the polyimides was done on a PL gel 5 μm mixed-C column. The mobile phase was HPLC grade THF with a rate of 5 mL per minute at 25°C. Polystyrene narrow molecular weight standards, by Fluka, ranging from 1,180 to 1,170,000 MW, were used to calibrate a PL-50 GPC (Agilent) with RI detector and PE LC200 chromatograph.

TABLE 1. Stoichiometric formulations of polyimides in mole fraction conformation.

Sample	Percent of EDR148 (PEO)	PMDA	BTDA	MBDMA	D230 (LPPO)	EDR148 (PEO)
PI-3	0%	0.50	N/A	0.10	0.40	0.00
PI-5	25%	0.50	N/A	0.10	0.30	0.10
PI-6	50%	0.50	N/A	0.10	0.20	0.20
PI-7	75%	0.50	N/A	0.10	0.10	0.30
PI-8	100%	0.50	N/A	0.10	0.00	0.40
PI-4	0%	N/A	0.50	0.10	0.40	0.00
PI-9	25%	N/A	0.50	0.10	0.10	0.30
PI-10	50%	N/A	0.50	0.10	0.20	0.20
PI-11	75%	N/A	0.50	0.10	0.30	0.10
PI-12	100%	N/A	0.50	0.10	0.00	0.40

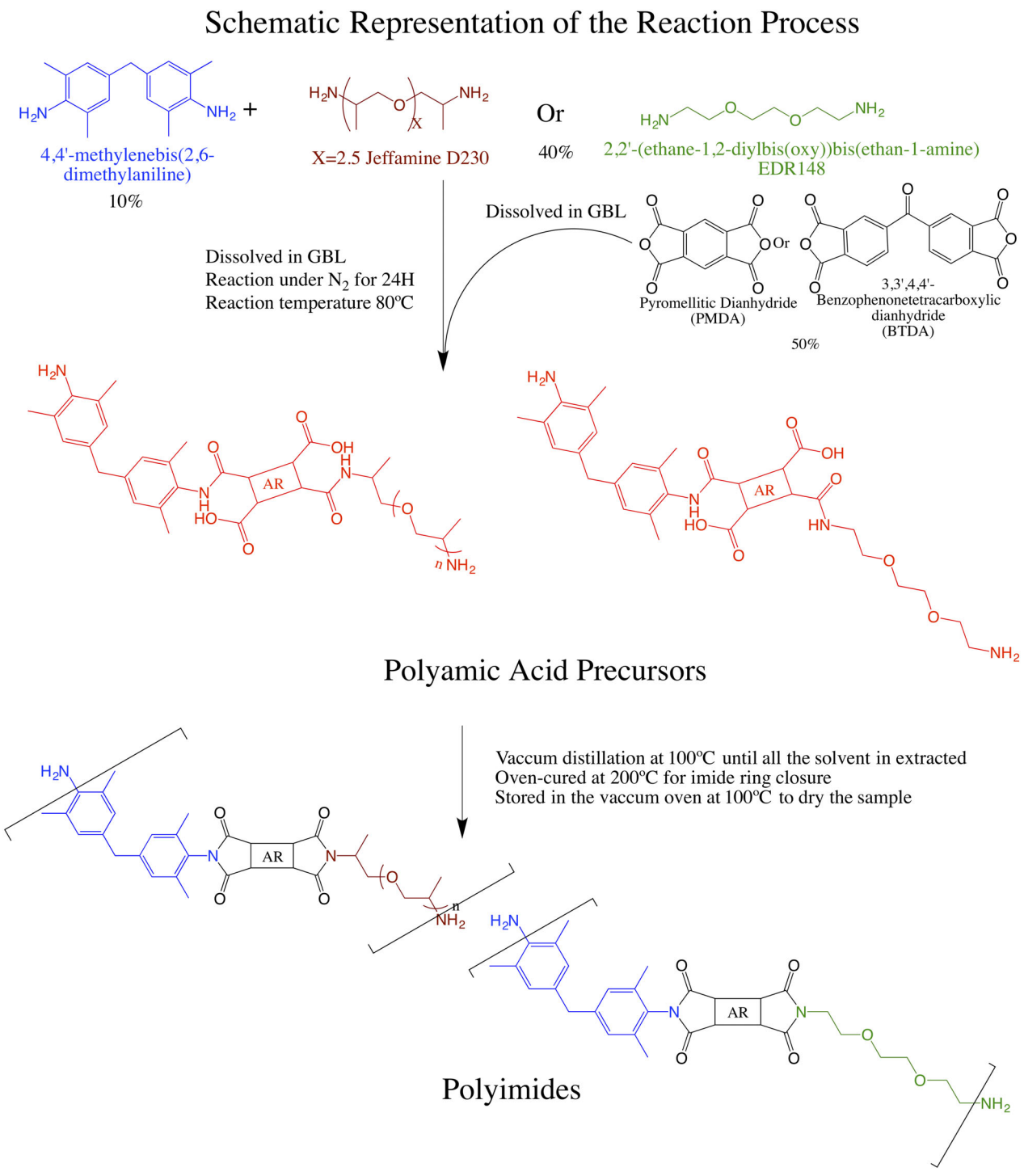

FIG. 1. Schematic representation of the polymerization of the polyimides. [Color figure can be viewed at wileyonlinelibrary.com]

Wide Angle X-Ray Scattering (WAXS). To investigate the degree of crystallization of synthesized polyimides, wide angle X-ray scattering WAXS was used. Films with a thickness between 0.1 and 0.2 mm were made using a Carver press. X-ray diffraction patterns were collected using Bruker D8 Advance theta-2theta diffractometer with copper radiation (Cu Kα, λ = 1.5406 Å) and a secondary monochromator operating at 40 kV and 40 mA, in the range of 2° and 70°, with a step of 0.020° at 25°C [35]. The samples were done on a Bruker D8 Advance using the DIFFRAC. COMMANDER software and the data was analyzed using a DIFFRAC.EVA V4.0.

Thermogravimetric Analysis (TGA). 25–30 mg samples from each polymer formulation were assayed for temperature stability with a TGA Q50 (TA Instruments) under nitrogen atmosphere. The samples were heated from 25°C to 600°C with a ramp rate of 10°C min^{-1}. The results were analyzed using the TA Data Analysis software.

Characterization of Glass Transition Temperature by Differential Scanning Calorimetry (DSC) and Dynamic Mechanical Analysis (DMA). Differential scanning calorimetry (DSC). Analysis was carried out using a DSC 2920 differential scanning calorimeter (TA Instruments) over the temperature range −30°C to 200°C. Temperature was calibrated using an Indium standard. The samples were cut and weighed; weights ranged from 9 to 10 mg. Samples were first heated from room temperature to 200°C at 20°C min^{-1}, cooled to −30°C at 20°C min^{-1}, and reheated to 200°C at 20°C min^{-1}. The cycle processes were used to erase thermal history due to sample preparation and storage. The results were analyzed using the TA universal analysis software and the second heating cycle was reported.

Dynamic mechanical analysis (DMA) was done on a rheometer AR2000 with a rectangular solid sample geometry. The samples (40 mm × 10 mm × 2 mm) were molded in a heated Carver hydraulic press at approximately 170°C with quick cooling to room temperature under 5 tons of pressure. Isothermal strain sweeps were performed on the rectangular samples to determine the linear viscoelastic regions (LVR) with an AR2000 rheometer (TA Instruments) at −50°C. The highest strain percent within the measured LVR was chosen to characterize the sample with a temperature ramp in oscillation mode. Ramp conditions were −100°C to 300°C at 10°C min^{-1} and 1 Hz with liquid nitrogen used for cooling. The information was collected in an AR2000 rheometer by TA instruments using the TA Rheology Advantage software. Resulting data were analyzed with the TRIOS software available from TA Instruments.

Dynamic Mechanical Analysis and Rheological Analysis for Activation Energy of T_g and Viscous Flow. Rectangular bars of 40 mm in length, 10 mm in width, and 2 mm in thickness were molded in a Carver press. The samples were used to measure the activation energy of the glass transition temperature (T_g). A time temperature superposition was made to calculate the activation energy using the Williams Landel Ferry model (WLF). A range of frequencies from 0.05 to 10 Hz at constant temperatures below and above the T_g of the sample (−20 to 200 °C in 5°C increments) were used. A common temperature of 120°C was selected to generate the master curve of the samples to compare the activation energies. The information was collected in an AR2000 rheometer with a rectangular solid sample geometry by TA instruments using a TA Rheology Advantage software and analyzed using a TRIOS software.

Discs of 25 mm in diameter and 3 mm in thickness were molded in a Carver press. The samples were used to measure the activation energy of the viscous flow. A time temperature superposition was made to calculate the activation energy using the Arrhenius model. A range of frequencies from 0.001 to 100 Hz at constant temperatures above the T_g of the sample (160 to 240°C in 10°C intervals) was used. A minimum of five different temperatures was used to create the master curve of the samples. A common temperature of 190°C was selected to create the master curve of the samples to compare the activation energies and the zero-shear viscosities. The information was collected in an AR2000 rheometer with 25 mm ETC plates by TA instruments using the TA Rheology Advantage software and analyzed using a TRIOS software.

Microhardness Testing. Discs of 25 mm in diameter and 3 mm in thickness were molded using a Carver press. The samples were secured inside a LEICA VMHT MOT Micro-Hardness Instrument. A center point was found, and the diamond indenter was used to mark a point on the sample. A load of 300 gf or 500 gf for a measurement duration of 15 s was applied for the indentation. Measurements for each sample were taken at room temperature. The indent was measured horizontally (D1mm) and vertically (D2). A total of five indentations were measured per side of the sample. The HV (MPa and kgf/mm^2) value was calculated and recorded as an indication of sample softness/hardness.

Tensile Testing. Films with a thickness between 0.1 and 0.2 mm were made using a Carver press. An ASTM D638 Type 5 die was used to cut the samples in the appropriate shape. Six dog-bone samples were cut out of each film and tested in the Shimadzu AGS-J. A 50 N force transducer (Model SM-50N-168) was used to test the samples. Each dog-bone was pulled at 25 mm per min. The average for the six trials was reported in the results. The results were recorded and analyzed using the TrapeziumX software.

RESULTS AND DISCUSSIONS

Infrared Spectroscopy and Proton Nuclear Magnetic Resonance

FTIR spectroscopy was conducted to prove that the polyamic acid precursor was successfully converted into a polyimide by the closure of the imide ring *via* imidization and to confirm the presence of the varying monomers that were added to the backbone. Complete imidization was confirmed with the absence of stretching vibrations of the O—H of carboxylic acid between 3,000 and 3,400 cm^{-1} and C═O of a secondary amide of the precursor at around 1,655 cm^{-1}. As seen in the spectra, the backbone of the neat samples and other polyimides had asymmetric and symmetric carbonyl vibrations characteristic of imides at around 1,770–1,773 cm^{-1} and around 1,702–1,711 cm^{-1} from the dianhydrides rings. The polyimides synthesized from PMDA had stronger carbonyl peaks than the polyimides composed from BTDA. Furthermore, all PI's had a C—O stretching vibration between 1,090–1,099 cm^{-1} that arose from the ether of the short polypropylene-oxide diamine (SPPO) monomer and a C═O bending vibration from the dianhydrides. The polyimides had an aromatic C═C stretching vibration at around 1,456 cm^{-1} which is derived from the dianhydride monomer. The presence of the polyethylene-oxide diamine monomer was confirmed with the C—N stretching vibrations of the amine moiety at 1352–1306 cm^{-1} and the C—O stretching vibrations of the ether functional group at 1236 cm^{-1}. The polyimide with BTDA had a stronger absorption band for the aromatic C═C stretching vibration, which was between 1,482 and 1,425 cm^{-1} since BTDA has an additional aromatic and an additional carbonyl in between the two aromatics. The C═O stretching vibration at around 1,671 cm^{-1} is attributed to the carbonyl found in BTDA. The C—N stretching vibration for the polyimide with BTDA ranged from 1,366–1,369 cm^{-1}. The C—N stretching vibrations for both types of polyimides with varying dianhydrides incremented as the stoichiometric ratio of polyethylene-oxide diamine were increased. Stretching vibrations for C—O was observed at about 1,293–1,247 cm^{-1}, which is from the ether of the polyethylene-oxide diamine.

The results of the peaks and regions are presented below:

PI-3: ATR-IR (cm^{-1}): 1770 cm^{-1} (asymmetric stretching C═O), 1,711 cm^{-1} (symmetric stretching C═O), 1,456 cm^{-1} (Ar—C═C stretching), 1,373–1,352 cm^{-1} (C—N stretching), 1,263 cm^{-1} (C—O stretching), 1,097 cm^{-1} (C—O stretching), and 729 cm^{-1} (C═O bending).

DOI 10.1002/pen

PI-5: ATR-IR (cm^{-1}): 1770 cm^{-1} (asymmetric stretching C═O), 1,711 cm^{-1} (symmetric stretching (C═O), 1,456 cm^{-1} (Ar—C═C stretching), 1,352–1,306 cm^{-1} (C—N stretching), 1,236 cm^{-1} (C—O stretching), and 727 cm^{-1} (C═O bending).

PI-6: ATR-IR (cm^{-1}): 1771 cm^{-1} (asymmetric stretching C═O), 1,708 cm^{-1} (symmetric stretching C═O), 1,456 cm^{-1} (Ar—C═C stretching), 1,356–1,312 cm^{-1} (C—N stretching), 1,237 cm^{-1} (C—O stretching), 1,099 cm^{-1} (C—O stretching), and 725 cm^{-1} (C═O bending).

PI-7: ATR-IR (cm^{-1}): 1772 cm^{-1} (asymmetric stretching C═O), 1,710 cm^{-1} (symmetric stretching C═O), 1,456 cm^{-1} (Ar—C═C stretching), 1,358–1,314 cm^{-1} (C—N stretching), 1,237 or 1,263 cm^{-1} (C—O stretching), 1,099 cm^{-1} (C—O stretching), and 725 cm^{-1} (C═O bending).

PI-8: ATR-IR (cm^{-1}): 1772 cm^{-1} (asymmetric stretching C═O), 1,710 cm^{-1} (symmetric stretching C═O), 1,456 cm^{-1} (Ar—C═C stretching), 1,358–1,314 cm^{-1} (C—N stretching), 1,237 or 1,263 cm^{-1} (C—O stretching), 1,099 cm^{-1} (C—O stretching), and 725 cm^{-1} (C═O bending).

PI-4 ATR-IR (cm^{-1}): 1773 cm^{-1} (asymmetric stretching C═O), 1,706 cm^{-1} (symmetric stretching C═O), 1,671 cm^{-1} (C═O stretching), 1,483–1,452 cm^{-1} (Ar—C═C stretching), 1,364 cm^{-1} (C—N stretching), 1,292–1,248 cm^{-1} (C—N stretching), 1,090 cm^{-1} (C—O stretching), and 726 cm^{-1} (C═O bending).

PI-9: ATR-IR (cm^{-1}): 1772 cm^{-1} (asymmetric stretching C═O), 1,705 cm^{-1} (symmetric stretching C═O), 1,673 cm^{-1} (C═O stretching), 1,484–1,427 cm^{-1} (Ar—C═C stretching), 1,367 cm^{-1} (C—N stretching), 1,293–1,247 cm^{-1} (C—N stretching), 1,090 cm^{-1} (C—O stretching), and 726 cm^{-1} (C═O bending).

PI-10: ATR-IR (cm^{-1}): 1772 cm^{-1} (asymmetric stretching C═O), 1,706 cm^{-1} (symmetric stretching C═O), 1,671 cm^{-1} (C═O stretching), 1,482–1,425 cm^{-1} (Ar—C═C stretching), 1,366 cm^{-1} (C—N stretching), 1,293–1,247 cm^{-1} (C—N stretching), 1,092 cm^{-1} (C—O stretching), and 725 cm^{-1} (C═O bending).

PI-11 ATR-IR (cm^{-1}): 1773 cm^{-1} (asymmetric stretching C═O), 1,706 cm^{-1} (symmetric stretching C═O), 1,671 cm^{-1} (C═O stretching), 1,483–1,426 cm^{-1} (Ar—C═C stretching), 1,368 cm^{-1} (C—N stretching), 1,293–1,246 cm^{-1} (C—N stretching), 1,094 cm^{-1} (C—O stretching), and 724 cm^{-1} (C═O bending).

PI-12 ATR-IR (cm^{-1}): 1773 cm^{-1} (asymmetric stretching C═O), 1,702 cm^{-1} (symmetric stretching C═O), 1,671 cm^{-1} (C═O stretching), 1,482–1,437 cm^{-1} (Ar—C═C stretching), 1,369 cm^{-1} (C—N stretching), 1,293–1,246 cm^{-1} (C—N stretching), 1,092 cm^{-1} (C—O stretching), and 724 cm^{-1} (C═O bending).

Gel Permeation Chromatography

Gel permeation chromatography (GPC) measurements yielded weight-average molecular weights (M_w) ranging from approximately 26,000 to 76,000 Da, number-averaged molecular weights (M_n) ranging from approximately 11,000 to 30,600 Da, and polydispersity indices (M_w/M_n) ranging from 2.08 to 2.71 (Table 2). The sample with a lower M_w and M_n was PI-7 (PMDA/75% PEO), and it might be due to being partially soluble in THF due to increase crystallinity. PI-8 and PI-12 which contained only PEO as an aliphatic amine were insoluble in THF. The polyethylene-oxide diamine increases the crystallinity of the polymer which reduces solubility.

TABLE 2. Molecular weight characterization of polyimides.

Sample	Percent of EDR 148	M_w	M_n	Polydispersity
PI-3	0%	49,310	22,271	2.2141
PI-5	25%	50,900	20,293	2.5083
PI-6	50%	76,396	30,677	2.4903
PI-7[b]	75%	26,243	11,189	2.3454
PI-8[a]	100%	N/A	N/A	N/A
PI-4	0%	38,511	18,496	2.0821
PI-9	25%	37,857	15,789	2.3977
PI-10	50%	40,510	140,949	2.7099
PI-11	75%	36,054	16,098	2.2397
PI-12[a]	100%	N/A	N/A	N/A

[a]The samples were not soluble in THF.
[b]Partially soluble in THF.

Wide Angle X-Ray Scattering (WAXS)

The arrangement of these monomers in a bulk polymer is controlled by chemical structure, three-dimensional orientation, and processing conditions [36]. Based on these factors, polymers could show amorphous or partially crystalline phase states. In a crystalline region, the organization of molecules is systematic conversely to the random orientation in the amorphous phase. Wide angle X-ray scattering provides a diffuse peak signal used to study amorphous polymers. These do not possess long-range order and thus consist of characteristically identifiable short-range order [37].

According to the obtained results, as shown in Fig. 2, only two samples from the PMDA series show defined peaks. In Fig. 2, PI-7 75% PEO and PI-8 100% PEO have five defined peaks in overlapping regions. The three common broad range peaks are existent in both samples and this could be related to the PMDA and MBDMA, which are held constant in both polymers. The other signals occur at lower 2θ values; the first one is not present for the PI-7 (75% PEO) sample and the second appears to be half the intensity, which could be representative of the influence of the orderly packing of the polyethylene-oxide diamine monomer. These diffused peaks are possible due to the local packing arrangement of the molecules. The results from the first run in the DSC confirm the presence of two different crystalline regions: one from 214°C to 216°C and the other from 249°C to 252°C (Fig. 3).

Thermogravimetric Analysis

Thermogravimetric analysis (TGA) was used to characterize the temperature stability (T_d) and possible solvent plus unreactive monomer retention of the polyimides. The samples were evaluated under a nitrogen atmosphere. The thermograms of the PIs are shown in Fig. 4. The resultant temperature at 5% weight loss and the onset temperature are described in Table 3. The diamine monomers and gamma butyrolactone used in processing have boiling points around 205°C, the minimal loss of mass around that temperature shows that the polymers were properly cured and dried. The stability at the onset temperature represents a relation between an ethylene oxide backbone (PEO) and a propylene

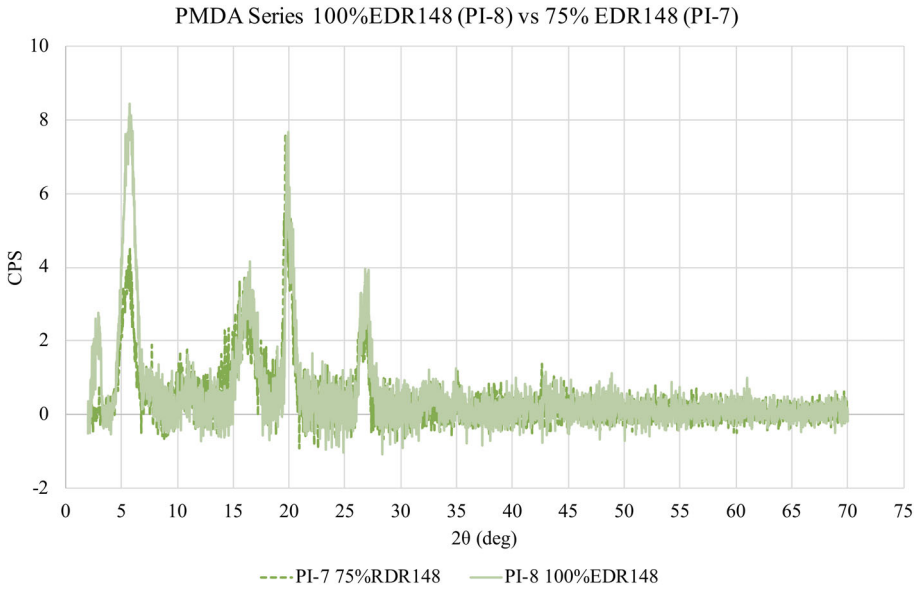

FIG. 2. WAXS of PI-7 and PI-8. [Color figure can be viewed at wileyonlinelibrary.com]

oxide backbone (SPPO). Conventional polyimides have higher temperature stability [5, 7] as their backbone is linear, well-ordered, rigid, and aromatic. Aromatic polyimides are recognized for having high thermal stability, but when the aromaticity is decreased with the incorporation of aliphatic monomers, the temperature stability decreases [19, 24]. The polyimides synthesized exhibit thermal onset stabilities that decrease as the glass transition temperatures decrease. The main variation in both series was the exchange from a polypropylene oxide diamine to a polyethylene oxide diamine. The change in monomers had the purpose of removing methyl pending groups and promoting the orderly packing of the chains [28–30].

In the BTDA series, it showed that with the increase in concentration of the polyethylene-oxide diamine the temperature stability increased. The T_d values ranged from 366°C to 384°C (Table 3). In the PMDA series, the trend continues where the temperature stability increased as the methyl pending groups in the polymer were reduced. The thermal stability T_d varied between 352°C to 381°C (Table 3). The crystallinity introduced increases thermal stability. The decomposition temperature (T_d) exceeded 350°C (Fig. 4) for all formulations, confirming that the monomer and solvent were eliminated during the curing and drying process. The information provided by TGA testing determines suitable temperature ranges for dynamic mechanical analysis and differential scanning calorimetry.

Characterization of Glass Transition Temperature by Differential Scanning Calorimetry (DSC) and Dynamic Mechanical Analysis (DMA)

The glass transition temperature (T_g) was measured by two different techniques, dynamic mechanical analysis (DMA) (Figs. 5 and 6) and differential scanning calorimetry (DSC) (Fig. 7). The

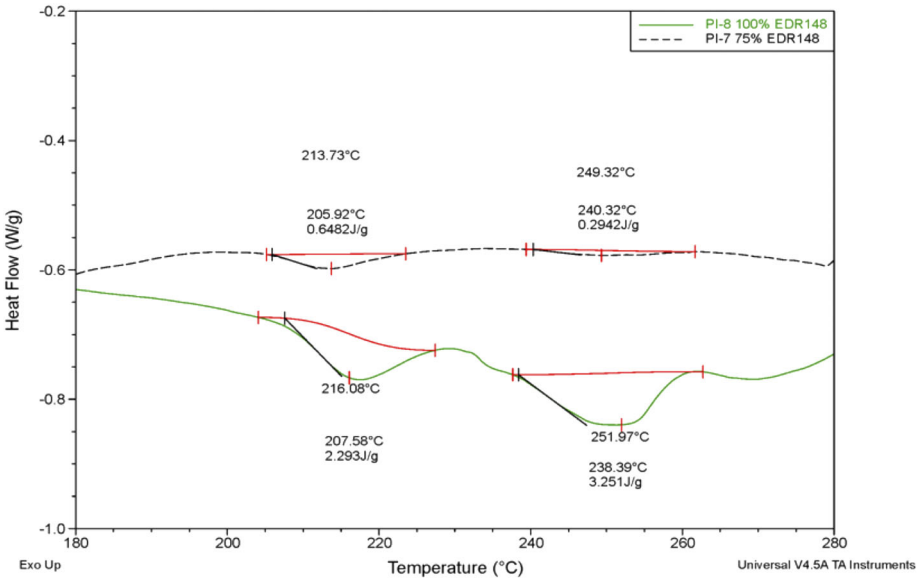

FIG. 3. DSC of PI-7 and PI-8. [Color figure can be viewed at wileyonlinelibrary.com]

 DOI 10.1002/pen

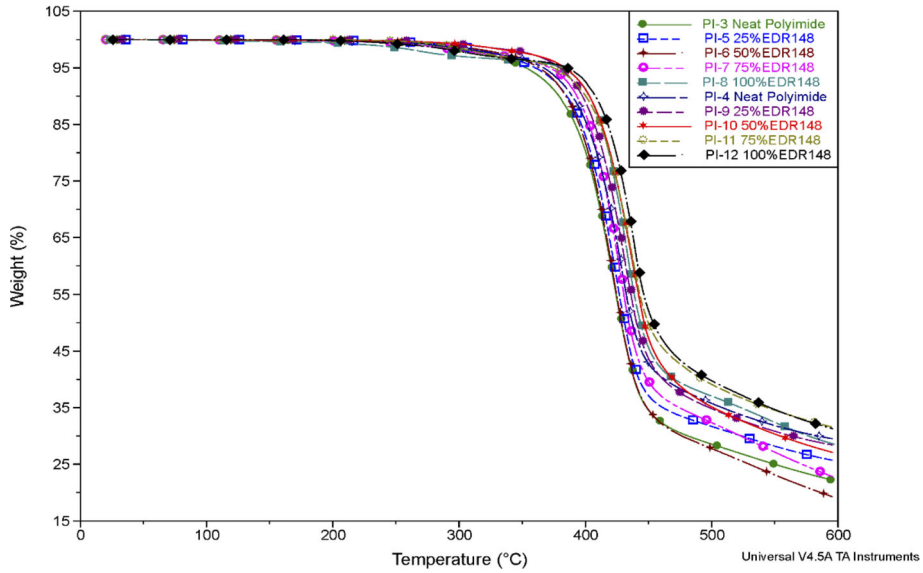

FIG. 4. Thermogram of polyimides based on PMDA and BTDA. [Color figure can be viewed at wileyonlinelibrary.com]

different techniques allowed a detailed characterization of this important transition. In the DMA, the T_g was taken from the peak of the alpha transition from the loss modulus G'' and the tan δ (Figs. 5 and 6). The T_g in the DSC manifests as a step decrease in the heat capacity of the polymer and will be defined here as the midpoint of the curve between the original baseline heat capacity and the resulting heat capacity (Fig. 7). At the three different temperatures, the polymer long chain segmental motion is measured by a change in the baseline of the DSC, an increase in the loss modulus before a large drop and finally an increase in the tan δ close to one in the ratio of the loss modulus G'' over the storage modulus G'. In this set of series, the main variation is the change of pending groups in the aliphatic linker to study the contribution to polyimides having lower transition temperatures but still perform as robust polyimides.

The glass transition temperatures in these polyimides are dominated by the absence of methyl pending groups in the aliphatic diamine and the organized packing between the polymer chains. The SPPO has a propylene oxide backbone while the PEO has an ethylene oxide backbone. The glass transition temperature varies from 77°C to 130°C from DSC (Fig. 7), 49°C to 99°C from G" and 69°C to 123°C from the loss factor tan δ (Figs. 5 and 6, Table 4). The common behavior regarding the glass transition is that as the backbone has less pending groups, the packing can be tighter which allows for a better organization and some crystalline regions can arise from this. The tighter packing allows for some physical stability in the sample above the T_g that leads to a large rubbery plateau (Figs. 5 and 6). These regions can be appreciated for the samples containing PMDA and PEO with a percentage of SPPO no greater than 25% of the monomer count. Some outlier to the trends, especially in the DMA method, must do with the combination between propylene oxide (SPPO) and ethylene oxide (PEO), which is due to the different structures that can organize well enough when they are alone but when mixed they create some void spaces in the packing. Due to the oscillatory movement in the DMA technique, the chain's slippage can start in those regions at lower temperatures. The behavior of the pending groups affects the T_g and the activation energy required to make the transition happen.

Dynamic Mechanical Analysis and Rheological Analysis and Activation Energy of T_g and Viscous Flow

Dynamic mechanical analysis was performed on rectangular solid samples under linear viscoelastic (LVE) strains determined from isothermal strain sweeps. Frequency sweeps at a constant temperature under these LVE-determined strains yielded transitions as frequency dependent increases of storage modulus G' and loss modulus G''. Different temperatures, starting below the glass transition until the sample lost its structure, were used to determine a broad range of storage modulus G' and loss modulus G'' at different temperatures and frequencies. Due to the constraints of the rectangular solid sample geometry, dynamic mechanical data after the glass transition (T_g) cannot be obtained because of a loss of rigidity and sample integrity within the geometry. The behavior of all the samples was common by having a large storage modulus G' close to 10^9 Pa when the temperature was below the T_g and the frequency was on the upper region of the measurement. At the end of the experiment, the moduli dropped 3 to

TABLE 3. Onset temperature and 5% loss.

Sample	Percent of EDR 148	Temperature at 5% loss (T_d) (ºC)	Temperature at onset point (°C)
PI-3	0%	352.77	373.95
PI-5	25%	360.18	379.01
PI-6	50%	363.12	378.40
PI-7	75%	371.56	380.81
PI-8	100%	381.05	396.72
PI-4	0%	366.82	379.77
PI-9	25%	379.61	388.89
PI-10	50%	383.90	390.04
PI-11	75%	374.21	404.91
PI-12	100%	384.55	400.75

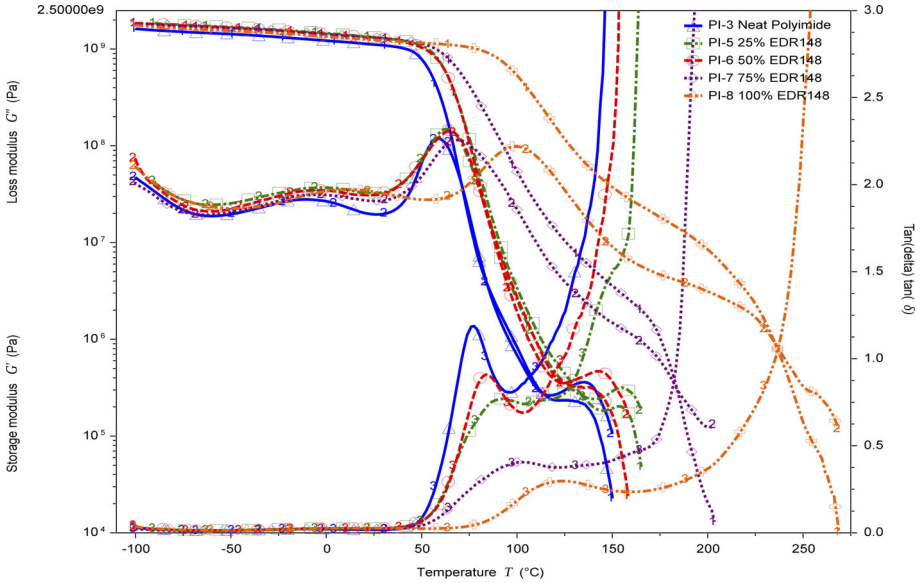

FIG. 5. Glass transition temperature of PMDA series (1 = G', 2 = G'', and 3 = tan δ). [Color figure can be viewed at wileyonlinelibrary.com]

4 orders of magnitude close to 10^5 Pa (Figs. 5 and 6); this was achieved at low frequencies and higher temperatures.

The study of the activation energy of the glass transition temperature was conducted using time temperature superposition (TTS) [38] (Fig. 8) and a Williams-Landel-Ferry plot (WLF) [39, 40] (Fig. 9). A common reference temperature, in the viscoelastic region of the single frequency temperature ramp, was selected. The reference temperature is typically situated between the glass transition temperature and T_g + 100°C since this interval is valid to apply the WLF equation [39–41]. The temperature selected was 120°C for all series. The TTS plot allows the creation of a master curve for each polymer composition. The WLF plot is then created from plotting the shift factor a_T [39–41], which represents the ratio of any mechanical relaxation time at temperature T to its value at a reference temperature T_0, with respect to temperature. The free space (f_g) and coefficient of thermal expansion (α_f) are used to define C_1 (B/2.303f_g) and C_2 (f_g/α_f).

$$Log(a_T) = \frac{-C_1(T-T_g)}{C_2+(T-T_g)} \quad (1)$$

From the fitting of the curve using the WLF equation is it possible to obtain the C_1 (B/2.303f_g) and C_2 (f_g/α_f) material constants [39, 40]. *Equation 2* was used to determine the activation energy [39, 40], ΔE_a:

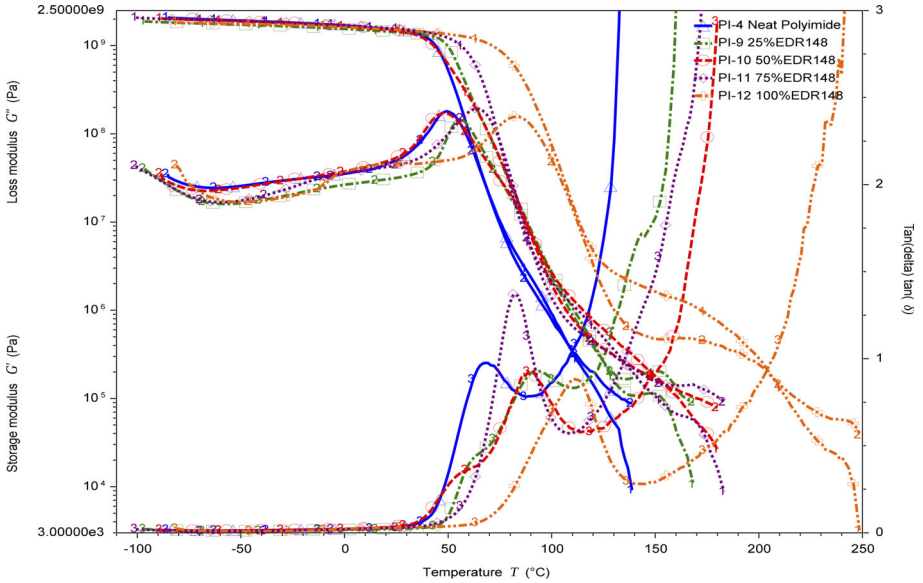

FIG. 6. Glass transition temperature of BTDA series (1 = G', 2 = G'', and 3 = tan δ). [Color figure can be viewed at wileyonlinelibrary.com]

 DOI 10.1002/pen

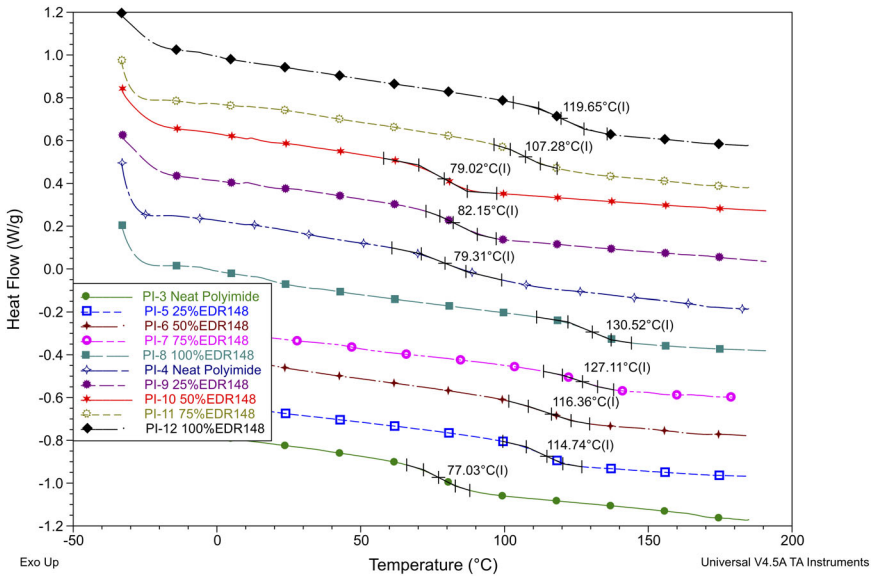

FIG. 7. Glass transition temperature of PMDA and BTDA series from DSC. [Color figure can be viewed at wileyonlinelibrary.com]

TABLE 4. Glass transition temperatures.

Series	Sample	Percent of EDR 148	T_g from tan (δ) (°C)	T_g from G'' (°C)	T_g from DSC (°C)	Storage modulus at −50°C
PMDA	PI-3	0%	77.45	59.47	77.03	1.43E+09
	PI-5	25%	91.81	63.77	114.74	1.69E+09
	PI-6	50%	83.82	64.39	116.36	1.66E+09
	PI-7	75%	104.95	68.28	127.11	1.65E+09
	PI-8	100%	123.94	99.09	130.52	1.54E+09
BTDA	PI-4	0%	69.24	49.17	79.31	1.92E+09
	PI-9	25%	91.80	55.29	82.15	1.73E+09
	PI-10	50%	90.90	47.82	79.02	1.89E+09
	PI-11	75%	81.54	63.28	107.28	1.91E+09
	PI-12	100%	110.53	82.15	119.65	1.76E+09

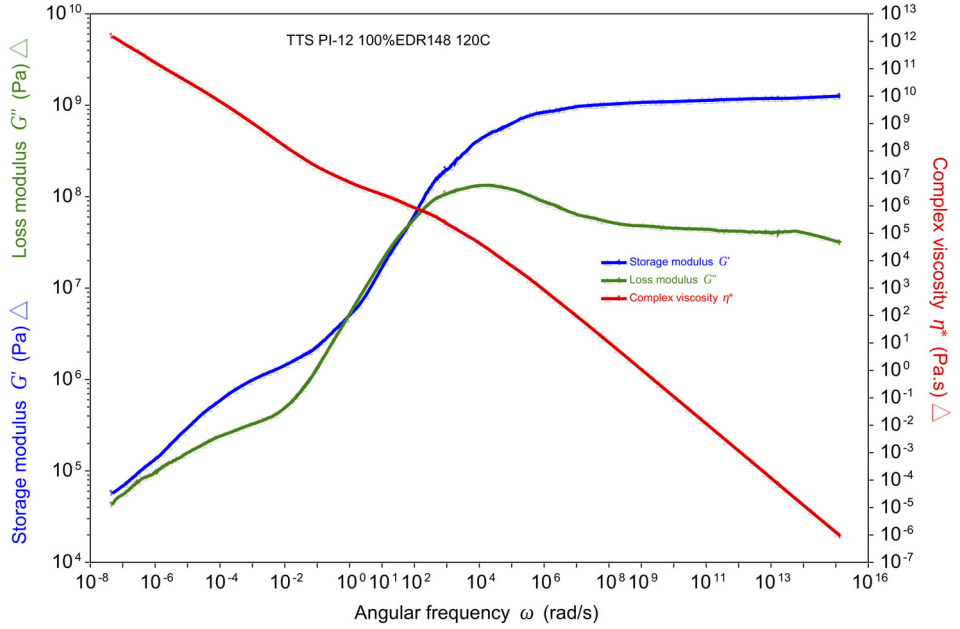

FIG. 8. Time–temperature superposition for the activation energy of the T_g of PI-12100%PEO. [Color figure can be viewed at wileyonlinelibrary.com]

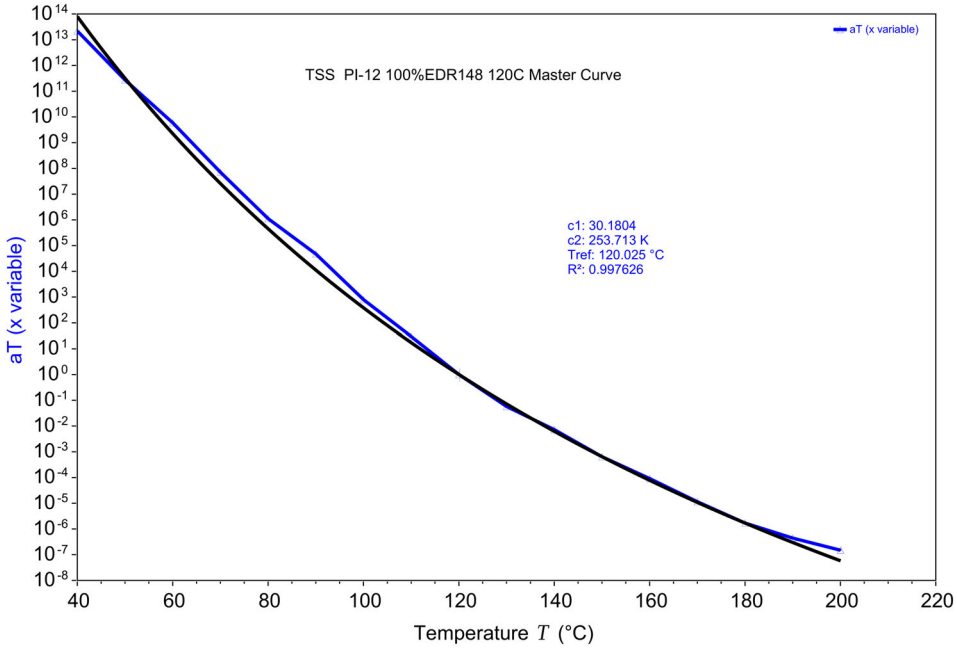

FIG. 9. WLF model for PI-12100%PEO. [Color figure can be viewed at wileyonlinelibrary.com]

$$\Delta E_a = 2.303\left(\frac{C_1}{C_2}\right)RT_g^2 \quad (2)$$

where R the universal gas constant, T is temperature and T_g is the glass transition temperature, all of them in Kelvin.

The activation energy of polymer chain near T_g region was lower than the samples that contained a major presence of methyl pending groups, which indicated that the introduction of crystalline regions increased the activation energy of polymer chain near T_g region. The results presented in Table 5 show that the C_1 constants varied from 10.0 to 47.4, the C_2 constants ranged from 128.7 K to 465.6 K [39], and the activation energies fluctuated from 173.1 to 369.2 kJ/mol. C_1 and C_2 vary from the universal constants of 17.4 and 51.6 K [39, 40]. This could be due to the three monomers that are interacting. Their different structures affect the fractional free volume and the thermal coefficient of expansion of the fractional free volume, which causes them to deviate from the standard.

The two flexible diamines were a factor that needed some consideration: SPPO has a propylene oxide backbone that incorporates short methyl groups grafted into the backbone and PEO has an ethylene oxide backbone. A similar trend is also apparent in the dianhydrides, the extra aromatic ring in the BTDA compared to the PMDA increases T_g and overall activation energies when keeping everything else the constant. The molecular weight of the sample can affect the T_g and consequently, the activation energy. Low molecular weight will not reach a critical entanglement point, which will lower the T_g subsequently the activation energy of the transitions [39]. The backbone contributed to a change in activation energy but the main influence was the impact of the methyl pendant groups added to the polymer and the influence in the tighter packing of the chains. The alignment order of the chains increases as the ethylene oxide content increases. When only the short polypropylene-oxide diamine (SPPO) or the polyethylene-oxide diamine (PEO) is present in the backbone the pattern is consistent and the repeating units can align in an organized manner. Once there is a mixture of the two monomers the packing is affected. In this case, the methyl pendant groups create void spaces. The C_1 and C_2 are related to the free space and coefficient of thermal expansion constants and their effects can be seen in the behavior of the polymers. When the free volume at T_g, f_g, increases the C_1 decreases and C_2 increases. As the amount of polyethylene-oxide diamine reaches 75% and 100% the ratio of

TABLE 5. Activation energy of T_g for polyimides.

Sample	Percent of EDR148 (PEO)	C1	C2 (K)	Reference temperature (K)	R^2	Activation energy of T_g (kJ/mol)
PI-3	0%	9.98	128.66	393.15	0.9984	229.50
PI-5	25%	14.46	163.05	393.15	0.9995	262.55
PI-6	50%	7.87	134.60	393.15	0.9990	173.12
PI-7	75%	47.45	465.63	393.15	0.9994	301.57
PI-8	100%	34.70	278.16	393.15	0.9945	369.19
PI-4	0%	28.99	250.72	393.15	0.9980	342.17
PI-9	25%	14.14	159.11	393.15	0.9953	263.04
PI-10	50%	23.87	215.13	393.15	0.9931	328.39
PI-11	75%	22.68	210.81	393.15	0.9981	318.45
PI-12	100%	30.18	253.71	393.15	0.9976	352.05

TABLE 6. Activation energy of viscous flow for polyimides.

Sample	Percent of PEO diamine	Activation energy of viscous flow (kJ/mol)	Reference temperature (K)	Zero shear viscosity (Pa·s)
PI-3	0%	142.22	463.15	849.692
PI-5	25%	166.55	463.15	1997.69
PI-6	50%	81.55	463.15	890.695
PI-7	75%	306.51	463.15	697,117
PI-8	100%	N/A	463.15	N/A
PI-4	0%	166.87	463.15	2,433.00
PI-9	25%	102.93	463.15	3,666.50
PI-10	50%	95.58	463.15	174,629
PI-11	75%	136.89	463.15	40,607.7
PI-12	100%	137.27	463.15	1,157,990

C_1 over C_2 increases due to a tighter packing and by consequence higher activation energy. The samples with 50% PEO in the PMDA series and the 25% PEO in the BTDA series have the lowest activation energy, which can be due to the interference of the two aliphatic diamine monomers creating free spaces between the chains, impeding an organized alignment. The activation energy is related to the T_g; with a high glass transition temperature, the activation energy needed to promote the slippage of the main chains needs to be greater. The overall pattern of the samples is shown below:

- PI-6 (50%) < PI-3 (0%) < PI-5 (25%) < PI-7 (75%) < PI-8 (100%) [PMDA]
- PI-9 (25%) < PI-11 (75%) < PI-10 (50%) < PI-4 (0%) < PI-12 (100%) [BTDA]

The activation energy is related to multiple factors that interfere with the movement of the chains and prevent their slippage. The different elements show constructive interference in the behavior of the activation energy of T_g. While this information is vital for the behavior of the material, most polymers are processed in a viscous form. Polyimides tend to have high thermal transitions and sometimes decompose before their rheological properties can be studied. The lower transitions of these polyimides allow the characterization of the viscous flow and the activation energy required for processing.

Polymers are usually molded into their final product using different techniques [42–45]. Each method requires a different set of parameters [44], but in the end, they are all related to the viscosity of the sample. The viscosity of a material can be influenced by shear rate, temperature, molar mass, or an external influence like a solvent. Rheological studies allow one to determine the characteristics of a polymer under processing conditions. *Equation 3* was used by the Trios software to calculate activation energy where $\log(aT)$ is the shift factor, E_a is the activation energy, R is the universal gas constant, T_0 is the initial temperature in Kelvin and T is the temperature in Kelvin [25].

$$2.303 \log(aT) = -\frac{E_a}{R}\left[\frac{1}{T_0} - \frac{1}{T}\right] \tag{3}$$

The Vogel-Fulcher-Tammann type *Eq. 4* was used to fit the temperature dependence of dynamic viscosity with given for constants, A_0 and T_0 [46]. It is then simplified to the *Eq. 5* to obtain E_a.

$$\ln(\eta) = \ln(A_0) + \frac{E_a}{R}\left(\frac{1}{T - T_0}\right) \tag{4}$$

$$\text{Slope} = T^* = \frac{E_a}{R} \tag{5}$$

The flow behavior of the polymers was clearly affected by the modifications incorporated into the backbone. The change from the propylene oxide to the ethylene oxide shows an increase in the zero-shear viscosity at 190°C. Therefore, the close packing of the chains results in an increase in viscosity. The sample with

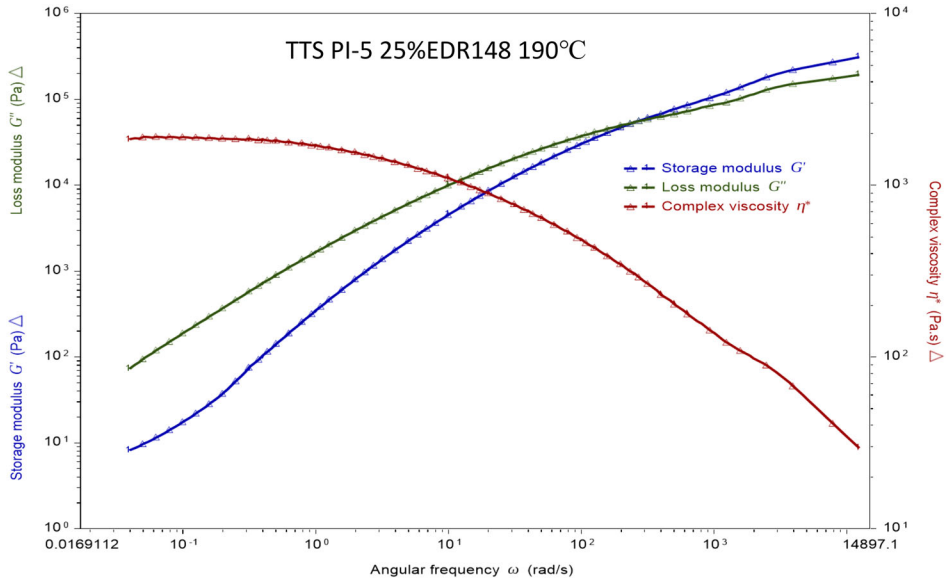

FIG. 10. Time–temperature superposition master curve for PI-5 25%PEO. [Color figure can be viewed at wileyonlinelibrary.com]

TABLE 7. Microhardness results for polyimides.

Sample	Percent of PEO diamine	d_1	d_2	HV (kgf/mm^2)	HV (MPa)
PI-3	0%	248.60 ± 4.93	249.40 ± 1.43	14.97 ± 0.33	146.8 ± 3.24
PI-5	25%	242.39 ± 11.2	240.87 ± 8.29	15.90 ± 0.69	155.9 ± 6.77
PI-6	50%	275.43 ± 8.00	273.28 ± 7.74	12.30 ± 0.66	120.6 ± 6.47
PI-7	75%	232.34 ± 10.4	233.26 ± 4.31	17.12 ± 0.91	167.9 ± 8.92
PI-8	100%	154.74 ± 6.27	151.28 ± 7.78	23.83 ± 1.64	233.7 ± 16.1
PI-4	0%	196.96 ± 5.76	198.21 ± 4.72	23.77 ± 0.82	233.1 ± 8.04
PI-9	25%	153.80 ± 3.00	158.40 ± 2.80	22.90 ± 0.50	224.6 ± 4.90
PI-10	50%	160.30 ± 3.90	170.20 ± 8.80	20.40 ± 1.10	200.1 ± 10.8
PI-11	75%	189.89 ± 7.46	194.82 ± 8.49	25.17 ± 1.77	246.8 ± 17.4
PI-12	100%	189.33 ± 2.55	191.26 ± 2.77	25.62 ± 0.55	251.3 ± 5.39

PMDA and 100% PEO did not flow at 190°C and is supported by DSC scans that reveal a crystalline region above the 190°C temperature (Fig. 3). The WAXS results (Fig. 2) also verify this behavior. The results from the rheological studies are used to determine the activation energy obtained *via* the time temperature superposition master curve, using the Arrhenius model. The activation energy depicts the influence of the methyl pending groups on chain packing. The mixture of the polyethylene-oxide diamine and the short polypropylene-oxide diamine creates void spaces in the polymer packing. This allows the flow to occur at lower temperatures or lower viscosities at a constant temperature. It can be seen in the low activation energies of both a one: one mixture of PEO and SPPO as void spaces in the packing reach the maximum (Table 6).

Extrusion molding is one of the common techniques used during the processing of polymer samples. This technique requires a viscosity of about 1,000 Pa·s [44], from the results in Fig. 10, the polyimides show that they can be processed above their T_g and below the T_d.

Microhardness

25 mm discs were indented multiple times on both sides of the sample to account for any morphological differences during the sample preparation. 2.94 N and 4.90 N (300 gf and 500 gf) were used as the indentation force to mark the samples and obtain a diamond shape pattern that was measured to obtain the hardness from *Eq. 6*. The results of the indentations are present in Table 7.

$$\mathrm{HV} = \frac{2F\sin\frac{136^\circ}{2}}{d^2} = 1.854\frac{F}{d^2} \tag{6}$$

Overall, the hardness is determined by the organized packing of the chains. The main variation of the polyethylene-oxide diamine shows a similar trend. The results of the presence of the methyl pending groups in the aliphatic component and how they affect the hardness of the polyimides are shown in Table 7. The hardness of the samples has a common dip in value for the sample that has equal amounts of the aliphatic amine with and without methyl pending groups. This could be due to a chain interaction that behaves as a void in the arrangement of the chains and creates some free space. The samples where the polyethylene oxide diamine (PEO) dominates have a higher HV value ranging from 168 to 234 MPa for PMDA, and 251 MPa for BTDA, while the samples where the short polypropylene oxide diamine (SPPO) dominates have a lower value ranging from 147 to 156 MPa for PMDA and 233 MPa for BTDA. The lowest HV hardness was seen for the 1:1 sample with a value of 120 MPa for PMDA and 200 MPa for BTDA. The tight packing of the chains creates a more compact material that is harder, while any free space disrupts the organization and lowers the hardness. The harder samples where the polyethylene-oxide diamine dominates are also the samples with higher T_g values, which shows the behavior of the pending groups in the overall properties of the polyimide.

Tensile Testing

The influence of crystalline regions on stress and strain values were observed for the polyimides formulations. When SPPO was combined with the BTDA and PMDA dianhydride, it made a flexible polymer [19]. After the introduction of PEO, there was a decrease in methyl pending groups from a polypropylene oxide

TABLE 8. Tensile testing results for polyimide samples.

Sample	Percent of PEO diamine	Stress at break (N/mm^2)	Strain at break (%)	Stress at max (N/mm^2)	Strain (%) at max	Young's modulus (N/mm^2)
PI-3	0%	28.15 ± 3.45	2.23 ± 0.50	28.15 ± 3.45	2.23 ± 0.50	18.26 ± 2.36
PI-5	25%	53.71 ± 2.56	3.69 ± 0.11	53.71 ± 2.56	3.69 ± 0.11	18.96 ± 1.86
PI-6	50%	34.95 ± 2.95	2.68 ± 0.14	34.95 ± 2.95	2.68 ± 0.14	19.20 ± 4.13
PI-7	75%	58.66 ± 4.47	3.69 ± 0.71	61.64 ± 2.83	3.92 ± 0.53	22.40 ± 1.90
PI-8	100%	67.32 ± 6.25	7.97 ± 2.09	67.32 ± 6.25	7.97 ± 2.09	17.01 ± 3.83
PI-4	0%	44.94 ± 6.28	2.36 ± 0.54	44.94 ± 6.28	2.36 ± 0.54	28.34 ± 5.86
PI-9	25%	44.13 ± 3.10	2.46 ± 0.38	44.13 ± 3.10	2.46 ± 0.38	22.42 ± 1.70
PI-10	50%	40.83 ± 5.55	3.56 ± 0.66	43.52 ± 3.63	3.39 ± 0.56	17.99 ± 3.02
PI-11	75%	50.49 ± 5.26	2.73 ± 0.46	50.49 ± 5.26	2.73 ± 0.46	23.44 ± 2.31
PI-12	100%	83.42 ± 7.75	3.94 ± 0.19	83.42 ± 7.75	3.94 ± 0.19	26.94 ± 3.15

diamine to a polyethylene oxide diamine; this increased the interaction between the chains and affected the tensile properties [47–49]. The results from the tensile test can be seen in Table 8. The tensile properties of the polymers are improved with the substitution of the short polypropylene-oxide diamine monomer for the polyethylene-oxide diamine monomer.

The behavior in both series is related to the dominance of the major linkage but differs in the strain trend. In the BTDA series first, the stress at max values ranged from 40 N/mm^2 to 83 N/mm^2. Secondly, the strain at max values ranged from 2.4% to 3.9%. In the PMDA series first, the stress values ranged from 28 N/mm^2 to 67 N/mm^2. Moreover, the strain values ranged from 2.2% to 8.0% (Table 8). In both cases, the uppermost stress and strain were achieved for the sample containing 100% PEO as the aliphatic monomer. The fracture of most of the samples was in the elastic strain region which explains the same values for ultimate tensile strength and fracture strength to be the same.

The results of the tensile testing support the indication that the polymer physical properties can be improved by promoting an orderly packing of the chains that could lead to crystalline regions within the polyimide. Compared to aromatic polyimides like Kapton® (DuPont), stress is only a fraction of what they can achieve, but the upper values of the 100% PEO samples are closer to Ultem® (G.E) while keeping the T_g at a lower temperature. The strain is highly improved, and it is all due to the aliphatic polyethylene-oxide diamine and the ability to crystallize from polyethylene oxide [29].

CONCLUSIONS

The effects of the methyl pending groups in the backbone are noticeable in the arrangement of the polymer chains. Fully aromatic polyimides are well known to exhibit high thermal stability and resistance to solvents, due to the interaction between the aromatic rings and the closed packing of the chains. The uniformity of the monomers allows for an organized packing into crystalline lattices. On the other hand, amorphous polyimides with aliphatic diamines have fewer interactions between the chains which lowers the thermal and physical stability that aromatic polyimides are praised for. The incorporation of the aliphatic polyethylene oxide diamines introduces a region in the backbone which increases the alignment of the polymer strands, which increases the interaction between the polymer chains. The processability compared to fully aromatic polyimides is improved and the thermal and physical stability compared to the aliphatic polyimides is enhanced. This works provides an expansion for aliphatic polyimides. By maintaining long chain aliphatic polyetherdiamines, we could impart flexible components into the backbone, making our polyimides melt processable using typical thermoplastic techniques, such as compression molding, injection molding, and extrusion. Thermal and mechanical properties, such as microhardness and decomposition temperatures, were also characterized. The larger forms processability of the material provides the elimination or reduction of the solvent used for the separator layer/electrolyte composite. The advantage of the flexible polyimide with a lower T_g comes from the manufacturing process because different options could be used and at lower energy expenses. The rheological analysis showed glass transition temperatures (T_g) ranging from approximately 69°C to 124°C according to tan δ peaks at 1 Hz and an increase in the rubbery plateau showing the improvement provided by crystalline regions. The flexible component came from the polyethylene oxide diamine monomer in the polyimide, which also works to provide the uniform sequence in the chain that allows the lattices that connect and hold the polymer above the T_g extending its range of usability.

ACKNOWLEDGMENTS

This research was supported through the generous donations of Jeffamine® D-Series diamines from Huntsman International LLC© and of solvents, monomers, and various consumables from Brightvolt©. The author would like to thank visiting researcher, Maxime Testemale, from L'École Nationale Supérieure de Chimie de Clermont-Ferrand for their collaboration during the testing and characterization of the polyimides.

REFERENCES

1. W. Qu, T.-M. Ko, R.H. Vora, and T.-S. Chung, *Polymer*, **42**(**15**), 6393 (2001).
2. A.L. Endrey, E.I. DU PONT DE NEMOURS AND COMPANY (United States of America). Polymeric compositions and process. CA 645073, issued 17 July 1962 (1962).
3. R. Hariharan, S. Bhuvana, M.A. Malbi, and M. Sarojadevi, *J. Appl. Polym. Sci.*, **93**(**4**), 1846 (2004).
4. Y. Han, X.Z. Fang, and X.X. Zuo, *Express Polym. Lett.*, **4**(**11**), 712 (2010).
5. A.C. Lua and J. Su, *Polym. Degrad. Stab.*, **91**(**1**), 144 (2006).
6. H. Yang, J. Liu, M. Ji, and S. Yang, *Novel Thermoplastic Polyimide Composite Materials*, INTECH Open Access Publisher, (2012).
7. L. Li, C. Guan, A. Zhang, D. Chen, and Z. Qing, *Polym. Degrad. Stab.*, **84**(**3**), 369 (2004).
8. M. Ghosh, *Polyimides: Fundamentals and Applications*, CRC Press, New York (1996).
9. Y. Han, X.-Z. Fang, and X.-X. Zuo, *High Perform. Polym.*, **22** (**8**), 989 (2010).
10. S. Xia, Z. Sun, L. Yi, and Y. Wang, *RSC Adv.*, **3**(**34**), 14661 (2013).
11. T. Namikoshi, K. Odahara, A. Wakino, M. Murata, and S. Watanabe, *High Perform. Polym.*, **27**(**2**), 183 (2014). https://doi.org/10.1177/0954008314542474.
12. T. Inoue, Y. Kumagai, M.-a. Kakimoto, Y. Imai, and J. Watanabe, *Macromolecules*, **30**(**7**), 1921 (1997).
13. Y. Kumagai, K. Itoya, M.A. Kakimoto, and Y. Imai, *J. Polym. Sci. A Polym. Chem.*, **38**(**8**), 1391 (2000).
14. N. Regnier and C. Guibe, *Polym. Degrad. Stab.*, **55**(**2**), 165 (1997).
15. M.A. Takassi, A. Zadehnazari, A. Farhadi, and S. Mallakpour, *Prog. Org. Coat.*, **80**, 142 (2015).
16. X. Pei, G. Chen, Y. Hou, and X. Fang, *High Perform. Polym.*, **25** (**3**), 312 (2013).
17. S. Takabayashi and M. Tooru. Method for producing polyimide film and polyamic acid solution composition. U.S. Patent 8,906,463, issued December 9, 2014 (2014).
18. K. Noda, C. Hiroki, S. Dai, and S. Kazuya. Method of producing polyimide resin, method of producing polyimide coating, method of producing polyamic acid solution, polyimide coating, and

polyamic acid solution. U.S. Patent 9,458,355, filed 20 August 2013 and issued 4 October 2016 (2013).

19. A. Rivera Nicholls, K. Kull, C. Cerrato, G. Craft, J.-.B. Diry, E. Renoir, Y. Perez, and J.P. Harmon, *Polym. Eng. Sci.*, **59**(**2**), 221 (2019). https://doi.org/10.1002/pen.24893.
20. S.-H. Hsiao, Y.-H. Hsiao, and Y.-R. Kung, *J. Electroanal. Chem.*, **764**, 31 (2016).
21. A. Kumar, S. Tateyama, K. Yasaki, M.A. Ali, N. Takaya, R. Singh, and T. Kaneko, *Polymer*, **83**, 182 (2016).
22. Y. Han, X.Z. Fang, and X.X. Zuo, *J. Mater. Sci.*, **45**(**7**), 1921 (2010).
23. K.B. Shepard, H. Gevgilili, M. Ocampo, J. Li, F.T. Fisher, and D. M. Kalyon, *J. Polym. Sci. B Polym. Phys.*, **50**(**21**), 1504 (2012).
24. A.F. Baldwin, R. Ma, C. Wang, R. Ramprasad, and G. A. Sotzing, *J. Appl. Polym. Sci.*, **130**(**2**), 1276 (2013).
25. K.L. Kull, R.W. Bass, G. Craft, T. Julien, E. Marangon, C. Marrouat, and J.P. Harmon, *Eur. Polym. J.*, **71**, 510 (2015).
26. G. Li, P. Li, H. Qiu, D. Li, M. Su, and K. Xu, *J. Biomed. Mater. Res. A*, **98**(**1**), 88 (2011). https://doi.org/10.1002/jbm.a.33100.
27. D.O. Corrigan, A.M. Healy, and O.I. Corrigan, *Int. J. Pharm.*, **235**(**1–2**), 193 (2002).
28. I.W. Hamley and M.J.J.L. Krysmann, *Langmuir*, **24**(**15**), 8210 (2008).
29. Y. Li, Q. Ma, C. Huang, and G. Liu, *Mater. Sci.*, **19**(**2**), 147 (2013). https://doi.org/10.5755/j01.ms.19.2.4430.
30. K. Pielichowski and K. Flejtuch, *Polym. Adv. Technol.*, **13** (**10–12**), 690 (2002). https://doi.org/10.1002/pat.276.
31. C.G. Wensley, A. Vallée, D. Brouillette, and S. Gustafson. Avestor LP and Solicore Inc. Polyimide matrix electrolyte. U. S. Patent 7,198,870, filed 29 July 2005 issued 3 April 2007 (2007).
32. C.G. Wensley, S. Gustafson, C.R. Nelson, R.W. Singleton, A. Vallee, and D. Brouillette. Avestor LP and Solicore Inc. Polyimide matrix electrolyte and improved batteries therefrom. U.S. Patent 7,129,005, filed 27 April 2005 and issued 31 October 2006 (2006).
33. H. Zhang and X. Wang, *Sol. Energy Mater. Sol. Cells*, **93**(**8**), 1366 (2009). https://doi.org/10.1016/j.solmat.2009.02.021.
34. J. Li, X. Yuan, S. Liu, Z. He, Z. Zhou, and A. Li, *ACS Appl. Mater. Interfaces*, **9**(**38**), 32643 (2017). https://doi.org/10.1021/acsami.7b07437.
35. G. Verma, S. Kumar, T. Pham, Z. Niu, L. Wojtas, J.A. Perman, Y.S. Chen, and S. Ma, *Cryst. Growth Des.*, **17**(**5**), 2711 (2017). https://doi.org/10.1021/acs.cgd.7b00198.
36. P. Sysel, *Encycl. Membr.*, **I**, 66 (2016).
37. H.G. Brittain, *Polymorphism in Pharmaceutical Solids*, CRC Press, New York (2016).
38. A. Oseli, A. Aulova, M. Gergesova, and I. Emri, *Mater. Today: Proc.*, **3**(**4**), 1118 (2016).
39. M.T. Shaw and W.J. MacKnight, *Introduction to Polymer Viscoelasticity*. 4th ed., John Wiley & Sons, Hoboken, NJ (2018).
40. J.J. Aklonis and W.J. Macknight, *Introduction to Polymer Viscoelasticity*, Amer Chemical Soc, Washington, DC (1984).
41. M.L. Williams, R.F. Landel, and J.D. Ferry, *J. Am. Chem. Soc.*, **77**(**14**), 3701 (1955).
42. J.D. Gander and A.J. Giacomin, *J. Polym. Eng. Sci.*, **37**(**7**), 1113 (1997).
43. M. Fleissner, *J. Int. Polym. Process.*, **2**(**3–4**), 229 (1988).
44. M. Gahleitner, *Prog. Polym. Sci.*, **26**(**6**), 895 (2001).
45. R. Fulchiron, A. Michel, V. Verney, and J. Roustant, *J. Polym. Eng. Sci.*, **35**(**6**), 513 (1995).
46. A. Messaâdi, N. Dhouibi, H. Hamda, F.B.M. Belgacem, Y. H. Adbelkader, N. Ouerfelli, and A.H. Hamzaoui, *J. Chem.*, **2015**, 1 (2015). https://doi.org/10.1155/2015/163262.
47. S. Sami, E. Yildirim, M. Yurtsever, E. Yurtsever, E. Yilgor, I. Yilgor, and G.L. Wilkes, *Polymer*, **55**(**18**), 4563 (2014). https://doi.org/10.1016/j.polymer.2014.07.028.
48. L. Ning, W. De-Ning, and Y.J.M. Sheng-Kang, *Macromolecules*, **30**(**15**), 4405 (1997).
49. S. Das, D.F. Cox, G.L. Wilkes, D.B. Klinedinst, I. Yilgor, E. Yilgor, and F. Beyer, *J. Macromol. Sci. B*, **46**(**5**), 853 (2007). https://doi.org/10.1080/00222340701388805.